

Temporal-MPI: Enabling Multi-Plane Images for Dynamic Scene Modelling via Temporal Basis Learning

Wenpeng Xing Jie Chen
Hong Kong Baptist University

November 23, 2021

Figure 1: Reconstruction quality demonstration of the proposed Temporal-MPI for the testing sequences from the multi-view video dataset [36]. Our method first learns a Temporal-MPI via supervisions from 12 synchronised multi-view videos recording a dynamic scene with 24 frames (extracted from longer video sequences). Given a query-time index during testing time, Temporal-MPI outputs an time-instance MPIs for only **0.002** seconds on one Nvidia Tesla V100 GPU, which is **3000** times faster, and with **3dB** higher average view-synthesis PSNR, than the *NeuralFlow* (CVPR21' [11]); and **1000** times faster, with **11** times less memory consumption, and **11dB** higher PSNR than the *3DMaskVol* (ICCV21' [12]). This enables real-time immersive novel-view synthesis for dynamic scene videos. The dynamic visual effects can be viewed in Adobe PDF Reader.

Abstract

Novel view synthesis of static scenes has achieved remarkable advancements in producing photo-realistic results. However, key challenges remain for immersive rendering for dynamic contents. For example, one of the seminal image-based rendering frameworks, the multi-plane image (MPI) produces high novel-view synthesis quality for static scenes but faces difficulty in modeling dynamic parts. In addition, modeling dynamic variations through MPI may require huge storage space and long inference time, which hinders its application in real-time scenarios. In this paper, we propose a novel Temporal-MPI representation which is able to encode the rich 3D and dynamic variation information throughout the entire video as compact temporal basis. Novel-views at arbitrary time-instance will be able

to be rendered real-time with high visual quality due to the highly compact and expressive latent basis and the coefficients jointly learned. We show that given comparable memory consumption, our proposed Temporal-MPI framework is able to generate a time-instance MPI with only **0.002** seconds, which is up to **3000** times faster, with **3dB** higher average view-synthesis PSNR as compared with other state-of-the-art dynamic scene modelling frameworks.

1 Introduction

Recent research advances on novel view synthesis have shown promising prospectus on immersive rendering of static scenes based on frameworks such as the Multi-plane

Images (MPI) [16, 34, 39] and the Neural Radiance Fields (NeRF) [4, 17]. Neural basis expansion [34] and Plenoc-tree structures [37] have been recently proposed to further improve the rendering quality. However, challenges still remain in modelling dynamic scenes, which require the additional capacity to capture the variation along the time dimension. To achieve this goal, efforts have been seen which add an additional time parameter as inputs to the NeRF model [10, 11, 23]. Although photo-realistic view-synthesis results can be produced by time-conditioned NeRF-style methods, it normally requires millions of times of ray-tracing during rendering, resulting in serious delay.

Another line of 3D content modelling method, the MPI, focuses on rendering real-world forward-facing contents. Without ray-tracing operations, it is highly efficient for real-time rendering. In order to render dynamic scenes using MPIs, pre-calculating and saving all time-instance MPIs is a straight-forward solution for time-space rendering. However, this method lacks temporal coherence and is expensive to save the bulky data incurred. *3DMaskVol21* [12] renders an image at a given timestamp by fusing a background MPI and instantaneous MPI with a 3D mask volume. Generating these three volumes causes around **2 seconds** delay. In comparison, our proposed method can generate arbitrary time-instance MPIs within **0.002 seconds**, which is much more efficient for real-time rendering applications.

In this paper, we propose a novel efficient representation for dynamic scenes, Temporal-MPI, for space-time immersive rendering. Different from previous methods [11, 12, 36] which rely on pre-trained optical flow model [6], ground-truth background images [12], pre-trained depth estimation model [24] or dynamic-static masks [36] as additional conditions, we aim at creating a self-contained pipeline. In addition, our method does not need to explicitly store time-instance MPIs, which greatly decreases the requirement for storage space. Computing time-instance MPIs based on the Temporal-MPI is highly computationally efficient.

2 Related Work

Novel view synthesis. View synthesis is a complex and long standing research issue that aims at synthesising novel views of a scene given arbitrary captured images, and has

become one of the most popular classes of research topics in computer vision. Early researches on Light fields (LF) [20] represented the scene as a 4D Plenoptic Function [15] $L(x, y, s, t)$, where (x, y) represents spatial coordinates and (s, t) represents angular coordinates. Then the spatial-angular correlations embedded in LF images are exploited for applications of depth estimation [7, 19], super-resolution [8] and novel view rendering [9, 29]. In addition to image based rendering and with recent advancements in deep learning, a grand of research using different forms of scene’s representations were proposed. The first branch of researches are using monocular input, such as *SynSin20* [33], *3D Photo20* [27], *WorldSheet21* [5] and *MPIs20* [32]. Above monocular methods all first predict scene’s geometry that is jointly learned with its renderer and color’s representations by back-propagating gradients from rendering loss. Then the novel view’s geometry that helps reveal occlusions and parallax structure can be reasoned and modeled with a reference to reference view’s geometry.

The second branch of research is using multi-view inputs that allow machine learning models to reason the scene’s geometry using epipolar geometry and ray tracing methods. Several differentiable scene representations were proposed to store and render the scene with continuous volumetric functions, such as Deep Voxels [28] and NeRF [17]. In addition to above continuous volumetric functions, a scene can be decomposed into a layered representation [26], such as MPI [39] and its followers [12, 16, 32, 34]. Although these methods can produce photo-realistic results, they can only model and render static scenes. The next key step of view rendering is rendering dynamic scenes.

Neural spatial and temporal embedding for novel-view synthesis. A successful novel view synthesis requires accurate modeling of a scene’s geometry. Modeling the geometry of non-rigid scenes with dynamic contents are ill-posed, and were tackled by reconstructing dynamic 3D meshes where priors like temporal information [1, 31] or known template configurations [2, 18] were fully exploited. Yet, these methods require 2D-to-3D matches or 3D point tracks. Thus, limiting their applicability to real world scenes or simulated scenes with complex textures.

Under the context of space-time view synthesis, adding time parameters to static scene’s representations is a straightforward implementation. Time conditioned warp-

ing fields [23], scene flow fields [11] and colors [10] are utilised in previous dynamic modeling methods. More specifically, *D-NeRF21* [23] added a time-conditioned deformation network to predict the time-dependent positional offsets to deform the canonical NeRF into a time-instance shape. *NeuralFlow21* [11] used temporal photometric consistency to encourage the time-conditioned NeRF to be learned from monocular videos. *Neural3DVideo21* [10] also transformed NeRF into a space-time domain, and achieved frame-interpolation by interpolating time-encoded latent vectors. However, the time-consuming rendering process of above NeRF-style methods limit their capabilities to real-time applications. Directly warping images to novel views according to depth is an efficient view-synthesis pipeline. *DynSyn20* [36] combined multi-view and single-view depths to generate temporal consistent depths for dynamic views warping. However, their method has two drawbacks: first, it requires foreground masks that separate static and dynamic contents; second, their method can not handle occlusions well. *3DMaskVol21* [12] proposed a method of generating dynamic MPI with a 3D mask volume to alleviate artifacts around the integration boundary of background and instantaneous MPIs. Yet, their method requires two-step training, and requires background images. Thus, limiting their general capabilities. Compared with NeRF-style methods, *DynSyn20* and *3DMaskVol21*, our method is efficient on rendering, end-to-end trainable and compact on storage.

Neural learnable basis. Our method is closely related to basis learning [13]. In signal processing, data often contains underlying structure that can be processed intelligently by linear combinations of *subspaces*. Tang et al. [30] learned subspace minimization for low-level vision tasks, such as interactive segmentation, video segmentation, optical flow estimation and stereo matching. PCA-Flow [35] predicted video’s optical flows as a weighted sum of the basis flow fields. We take inspiration from these works, and learn coefficients to combine globally shared time-wise subspaces to draw instantaneous MPIs.

3 Approach

Given a set of synchronized multi-view videos of a dynamic scene $\{\mathbf{I}_t^k\}$, where $t = 1, 2, \dots, T$ and $k = 1, 2, \dots, K$ are the frame number and camera indices, respectively,

our goal is to construct a *compact* 3D representation which enables *real-time* and *novel-view* synthesis of the dynamic contents at *any* given time $t \in [1, T]$. To achieve the goal, one naive option is to calculate and save a separate MPI for every video frame, $\mathcal{M} = \{\mathbf{M}_t \in \mathbb{R}^{H \times W \times D \times 4}\}_{t=1}^T$. This however, will be extremely memory- and computation-inefficient (generating \mathcal{M} incurs more than $225 \times T$ MB data and around 2 seconds delay when rendering at VGA resolution [12]). As such, rather than having to calculate and save MPIs for all video frames in advance or having to calculate an MPI on-the-run, we investigate a novel Temporal-MPI representation with learned temporal basis to compactly encode dynamic variation throughout the entire video. An overall pipeline of our approach is shown in Figure 2.

In the following, we will first briefly introduce the vanilla MPI representation in Section 3.1. The temporal basis formulation will be elaborated in Section 3.2, and the novel-view temporal reconstruction will be explained in Section 3.3.

3.1 The Multi-plane Image Representation

Being one of the seminal representation frameworks for 3D content embedding and novel-view synthesis, Multi-plane Images (MPI) learn layered depth composition of the scene from a set of multi-view references [16, 39, 39]. Let D denote the number of depth layers in a MPI, with the dimension of each layer being $H \times W \times 4$, where H and W denote the height and width of the MPI layers, respectively.

An MPI representation $\mathbf{M} = \{\mathbf{C}_d, \mathbf{A}_d\}_{d=1}^D$ is composed of multiple layers of 3-channel RGB images $\mathbf{C}_d \in \mathbb{R}^{H \times W \times 3}$ and one-channel alpha images $\mathbf{A}_d \in \mathbb{R}^{H \times W \times 1}$, where d denotes the depth plane index.

Synthesizing novel-views $\hat{\mathbf{I}}$ based on the MPI \mathbf{M} involves two steps: first, warp all depth planes in the MPI homographically from the reference view to the target view; and second, render pixels using alpha-composition [22] over each layer’s color:

$$\hat{\mathbf{I}} = \mathcal{O}(\mathcal{W}(\mathbf{A}), \mathcal{W}(\mathbf{C})), \quad (1)$$

here \mathcal{W} denotes the warping operator, and \mathcal{O} denotes the

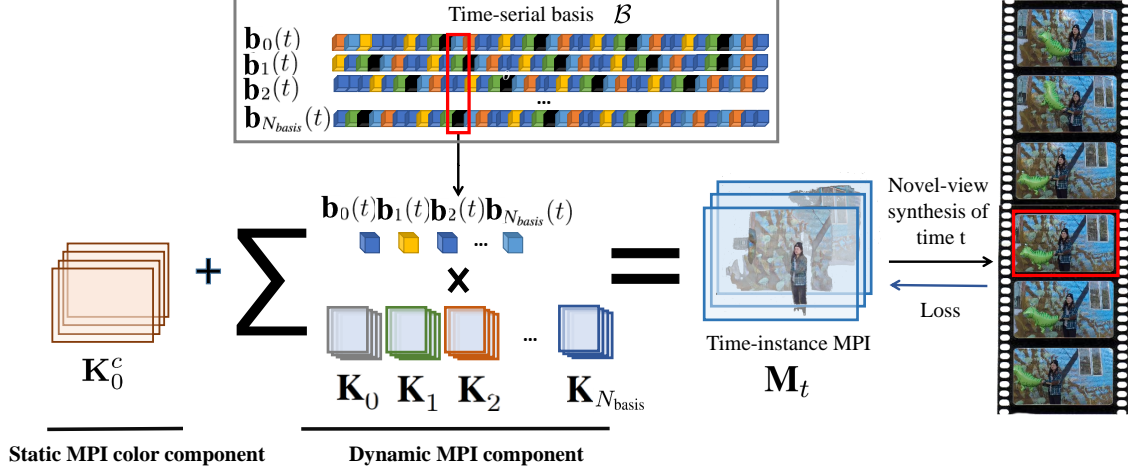


Figure 2: Overall pipeline. The proposed Temporal-MPI contains three parts: static component \mathbf{K}_0^c , temporal basis \mathcal{B} and dynamic coefficients $\{\mathbf{K}_n\}_{n=1}^{N_{\text{basis}}}$. The alpha and color values in instantaneous MPI \mathbf{M}_t are recovered as linear combinations of bases and adding static component \mathbf{K}_0^c from Temporal-MPI $\hat{\mathcal{M}}$. The color in the corresponding frame is rendered as MPI’s alpha composition in Equation 1. The overall pipeline is end-to-end differentiable and supervised by pixel rendering loss. Due to limitations of GPU memory, above operations are conducted in units of a batch of rays.

compositing operator, and it is defined as:

$$\mathcal{O}(\mathbf{A}, \mathbf{C}) = \sum_{d=1}^D \mathbf{C}_d \mathcal{T}_d(\mathbf{A}), \quad (2)$$

$$\mathcal{T}_d(\mathbf{A}) = \mathbf{A}_d \prod_{i=d+1}^D (1 - \mathbf{A}_i). \quad (3)$$

Both the composition \mathcal{O} and the warping \mathcal{W} operations are differentiable, thus allowing the representation \mathbf{M} to learn the geometry and color information from final pixel rendering loss.

3.2 Temporal Basis Formulation

At a given time instance $t \in [1, T]$, we denote the MPI that can be calculated based on the multi-view references as \mathbf{M}_t . For the entire video sequence, an MPI-video can be generated as: $\mathcal{M} = \{\mathbf{M}_t \in \mathbb{R}^{H \times W \times D \times 4}\}_{t=1}^T$. Based on the afore-analyzed reasons, we cannot exhaustively calculate and save \mathcal{M} . We propose a novel Temporal-MPI representation which is able to encode the rich 3D and dynamic variation information throughout the entire

video as compact temporal basis, and in the meantime, preserve high rendering efficiency for real-time novel-view synthesis. To achieve this, we divide the goal into two tasks, i.e., (i) learning of the static background as explicit parameters, and (ii) learning of the dynamic variation over a set of temporal basis.

3.2.1 Explicit Parameter Learning for Static Background

Static contents in a video constitute the low-frequency part of the total energy along the time dimension, which can be well-captured and modeled explicitly by time-invariant parameters. By treating all the frames of the multi-view video $\{\mathbf{I}_t^k\}_{t,k}$ as reference views equally and ignoring their respective frame indices, we can directly learn the multi-plane RGB color parameters $\mathbf{K}_0^c \in \mathbb{R}^{H \times W \times D/8 \times 3}$ using the pixel rendering loss. \mathbf{K}_0^c models the low-frequency energy of the video, with possible blur over the dynamic area. Such an explicit modelling scheme for the static component proves to be important [34] and let the subsequent dynamic modelling to better focus on the temporal variation.

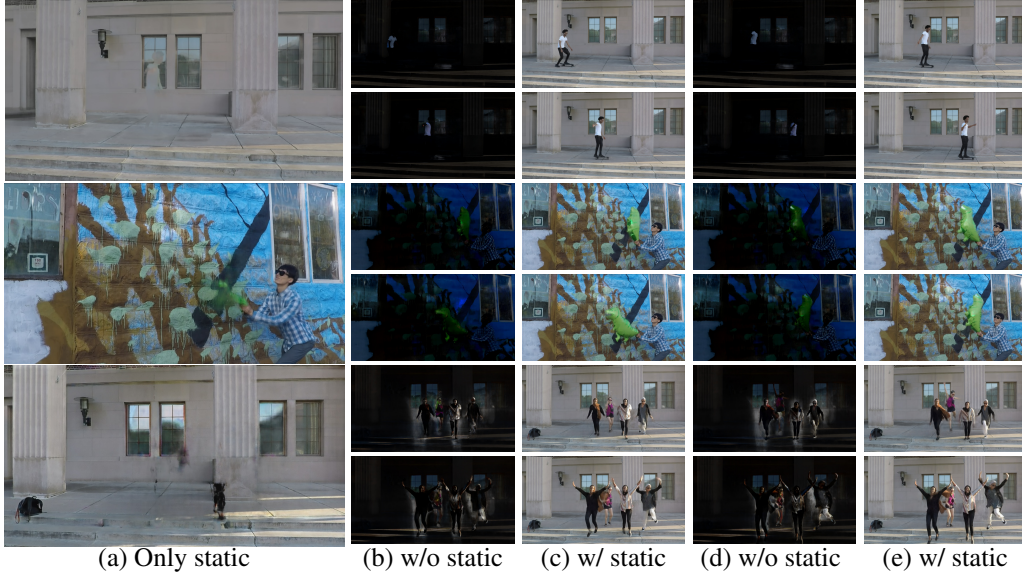


Figure 3: Static scene representation ablation study. The static components are rendered in (a); color output from the dynamic components are rendered in (b) and (d); full rendering are visualised in (c) and (e).

Table 1: Comparison on real-time rendering/inference speed and output resolution. The data of time-usage are referenced from their original papers. We assume the length of the modeled dynamic video is 24 frames. *3DMaskVol21* will require 24 MPIs for real-time rendering of the whole sequence. *NeuralFlow21* is impossible for real-time tasks.

Methods	<i>NeuralFlow21</i>	<i>3DMaskVol21</i>	Ours
Inference Time (seconds, ↓)	6.00	2.03	0.002
Output Resolution(pixel, ↑)	512×288	640×360	576×300
Network Parameters (million, ↓)	5.26	1.17	6.00
Storage Space (Mb, ↓)	–	$225 \times 24 = 5400$	481

3.2.2 Temporal Basis Learning for Dynamic Contents

Compared with a static background, the dynamic contents in \mathcal{M} constitute the high-frequency energy along the time dimension. Being high-dimensional and with dynamic variations, the dynamic contents still constitute a highly regularized manifold, considering the fact that (i) the video length is limited (we model video with 24 frames in length, although these frames could be extracted from longer video sequences), and (ii) dynamic pixels within a scene usually show consistent motion in clusters. This motivates us to compactly represent the dynamics based on a few learned

temporal basis.

We denote the temporal basis as $\mathcal{B} \in \mathbb{R}^{4 \times T \times N_{\text{basis}}}$ which span the temporal variation space for \mathcal{M} . Here N_{basis} denotes the total number of basis. The first dimension of \mathcal{B} is set to 4 which is reserved for modelling both the MPI color component (with 3 channels): $\mathcal{B}^c = \{\mathbf{b}_n^c\}_{n=1}^{N_{\text{basis}}}$, and the alpha component $\mathcal{B}^\alpha = \{\mathbf{b}_n^\alpha\}_{n=1}^{N_{\text{basis}}}$ (one channel). Therefore $\mathcal{B} = [\mathcal{B}^c, \mathcal{B}^\alpha]$.

In our proposed framework, the temporal basis will be estimated by two time-dependent functions which are

Multi-Layer Perceptron (MLP) networks \mathcal{V}^c and \mathcal{V}^α :

$$\{\mathbf{b}_n^c(t)\}_{n=1}^{N_{\text{basis}}} = \mathcal{V}^c(\mathcal{E}(t)) : \mathbb{R} \mapsto \mathbb{R}^{3 \times N_{\text{basis}}}, \quad (4)$$

$$\{\mathbf{b}_n^\alpha(t)\}_{n=1}^{N_{\text{basis}}} = \mathcal{V}^\alpha(\mathcal{E}(t)) : \mathbb{R} \mapsto \mathbb{R}^{1 \times N_{\text{basis}}}. \quad (5)$$

Here $\mathcal{E}(\cdot)$ is a time-encoding function which encodes time-sequential information into a high dimensional latent vector [10]. The temporal basis \mathcal{B} learns a parsimonious frame that efficiently spans the temporal variation manifold. With a *pixel-specific* coding coefficient (to be elaborated in the next section), \mathcal{B} can efficiently model the MPI pixel’s temporal variation throughout the entire video.

3.3 Temporal Coding for Novel-view Synthesis

For an arbitrary frame index $t \in [1, T]$, a time-instance MPI $\mathbf{M}_t = [\mathbf{A}_t, \mathbf{C}_t]$ can be constructed based on the temporal basis \mathcal{B} according to:

$$\mathbf{C}_t(\mathbf{x}) = \mathbf{K}_0^c(\mathbf{x}) + \sum_{n=1}^{N_{\text{basis}}} \mathbf{K}_n^c(\mathbf{x}) \times \mathbf{b}_n^c(t), \quad (6)$$

$$\mathbf{A}_t(\mathbf{x}) = \sum_{n=1}^{N_{\text{basis}}} \mathbf{K}_n^\alpha(\mathbf{x}) \times \mathbf{b}_n^\alpha(t). \quad (7)$$

Here $\mathbf{K}_n^\alpha(\mathbf{x})$ and $\mathbf{K}_n^c(\mathbf{x})$ are the coding coefficients for the respective temporal basis at a given MPI spatial location $\mathbf{x} \in \mathbb{R}^3$ (the 3 dimensions of \mathbf{x} include its 2D coordinates and the depth plane index in \mathcal{M}_t). These coding coefficients are estimated by another set of MLPs \mathcal{K}^c and \mathcal{K}^α :

$$\{\mathbf{K}_n^c(\mathbf{x})\}_{n=1}^{N_{\text{basis}}} = \mathcal{K}^c(\mathcal{R}(\mathbf{x})) : \mathbb{R}^3 \mapsto \mathbb{R}^{3 \times N_{\text{basis}}}, \quad (8)$$

$$\{\mathbf{K}_n^\alpha(\mathbf{x})\}_{n=1}^{N_{\text{basis}}} = \mathcal{K}^\alpha(\mathcal{R}(\mathbf{x})) : \mathbb{R}^3 \mapsto \mathbb{R}^{1 \times N_{\text{basis}}}. \quad (9)$$

Similarly, here $\mathcal{R}(\cdot)$ is a position-encoding function which encodes the spatial information \mathbf{x} into high-dimensional representations [17].

Based on Equation (6) and (7), the time-instance MPI \mathbf{M}_t can be warped and composited to any arbitrary viewing angles according to Equation (2) and (1). In addition, by querying all elements $t = 1, \dots, T$ along the temporal basis, we can construct the time-instance MPI for all video frames.

Remarks. (i) our proposed temporal MPI representation composes of an explicitly learned static multi-plane color component $\mathbf{K}_0^c \in \mathbb{R}^{H \times W \times D/8 \times 3}$, and a dynamically coded dynamic component via simultaneous basis and co-efficient learning. We have achieved compression along the temporal dimension via the temporal basis, which compactly encodes dynamic color and geometry variation information throughout the entire video. $\mathbf{K}_0^c(x)$ is interleaved by 8 times in depth dimension when selected by a batch of rays, the post-repetition can decrease the size of \mathbf{K}_0^c , and thus saving GPU memory in storing \mathbf{K}_0^c .

(ii) To maintain rendering efficiency and save storage-space, spatial-temporal information is efficiently encoded and propagated among different components in the Temporal-MPI. First, the static component \mathbf{K}_0^c is temporally shared among all time frames, this ensures overall reconstruction quality and enables the dynamic components to focus on variations only; and second, the dynamic coefficients, i.e., $\{\mathbf{K}_n^c(\mathbf{x})\}_{n=1}^{N_{\text{basis}}}$ and $\{\mathbf{K}_n^\alpha(\mathbf{x})\}_{n=1}^{N_{\text{basis}}}$, are point-wisely coded/learned, however, over a common set of temporal basis. This helps to remove the redundancy in modelling dynamic variation, and also helps to remove motion ambiguities for some pixels.

3.4 Training Loss Function

To let the Temporal-MPI focus on reconstruction quality, we ignore the sparsity of coding coefficients for this task. Coefficients and the temporal basis are jointly learned and optimised. The whole system will be optimised via the following loss function \mathcal{L} :

$$\mathcal{L} = \|\hat{\mathbf{I}}_t^k - \mathbf{I}_t^k\|_2 + \lambda_1 \|\nabla \hat{\mathbf{I}}_t^k - \nabla \mathbf{I}_t^k\|_1 + \lambda_2 \text{TVC}(\mathbf{K}_0^c), \quad (10)$$

where $\hat{\mathbf{I}}_t^k$ is the rendered image at time t for the camera k , \mathbf{I}_t^k is the ground truth image from the same view. The first term in \mathcal{L} calculates the L_2 reconstruction loss. The second term penalises edge inconsistencies, with ∇ denoting the gradient operator. In the third term, TVC denotes total variation loss [3]. λ_1 and λ_2 are balancing weights for different loss terms.

4 Experiments

4.1 Implementation Details

Our model is implemented in PyTorch 1.10, using Adam as optimiser and querying 15000 rays in a batch forward. The initial learning rate is set as 0.001, and decay by 0.1 every 2000 steps. The model takes three days to be trained for 800 epochs on one Nvidia Tesla V100 GPU. The output resolution is 576×300 . The position-encoding method in [17] is formulated as $\mathcal{R}(p) = [\sin(2^0 \frac{\pi}{2} p), \sin(2^0 \frac{\pi}{2} p), \dots, \sin(2^l \frac{\pi}{2} p), \cos(2^l \frac{\pi}{2} p)]$ where the input location of scene point is normalised to $[-1, 1]$ and l is the index of encoding level set as 3. The index of time is embedded into a latent vector in size of 32 using dictionary learning as in [10]. For networks that parameterise \mathcal{K}^c and \mathcal{K}^α , we use MLP networks with 8 layers and 384 hidden nodes. Networks for \mathcal{V}^c and \mathcal{V}^α are using MLP with 4 layers and 64 hidden nodes. The shape of dynamic coefficients $\{\mathbf{K}_n^c(\mathbf{x})\}_{n=1}^{N_{\text{basis}}}$ and $\{\mathbf{K}_n^\alpha(\mathbf{x})\}_{n=1}^{N_{\text{basis}}}$ in Temporal-MPI is $320 \times 596 \times 32 \times 4 \times 5$ where 32 is the number of plans D , 596 and 320 are width W and height H including marginal offsets set as 10, 4 includes 3 channels of colors and 1 channel of alpha, and 5 is the number of basis N_{basis} . The shape of temporal basis \mathcal{B} is $4 \times 5 \times 24$ where 5 is the number of basis N_{basis} , 24 is the total number of timestamps and 4 includes 3 channels for color and 1 channel for alpha. Static component \mathbf{K}_0^c is in the shape of $320 \times 596 \times 4 \times 3$ before the repetition along depth dimension.

4.2 Dataset

Our model is trained and evaluated on the Nvidia Dynamic Scenes Dataset [36] that contains 8 scenes with motions recorded by 12 synchronized cameras. Their camera parameters are estimated using COLMAP [25]. We extracted 24 frames from the video sequence, and used multi-view images in selected frames for training, but leaving 1 held-out view as a test view in each timestamp.

4.3 Ablation Study

In this section, we investigate the effectiveness of our main contributions in Temporal-MPI: dynamic coefficient, temporal basis and static component.

4.3.1 Number of Basis

We investigate the relationships between rendering quality and number of basis N_{basis} . From the results in Table 2, we can find the positive relationships between N_{basis} and PSNR. But the results of PSNR flatten when the N_{basis} is bigger than 5. On the other hand, N_{basis} determines the size of $\{\mathbf{K}_n^c(\mathbf{x})\}_{n=1}^{N_{\text{basis}}}$, $\{\mathbf{K}_n^\alpha(\mathbf{x})\}_{n=1}^{N_{\text{basis}}}$ and \mathcal{B} that affects storage size. So in order to research a balance between rendering quality and compression rate, we select N_{basis} as 5.

Table 2: Ablation study on PSNR vs. number of basis.

Scene/PSNR	Number of basis						
	1	3	5	7	9	11	13
Skating-2	33.5	35.4	36.2	36.3	36.8	37.4	36.6

4.3.2 Video Length

We evaluate the performance of our model trained with different lengths of video. As shown in Table 3, We found performance degradation when the total number of timestamps T increased. This is due to reaching the representation threshold of temporal basis and dynamic coefficients.

Table 3: Ablation study on PSNR vs. total number of timestamps.

Scene/PSNR	Number of timestamps						
	8	16	24	32	40	48	60
Skating-2	37.8	37.6	36.2	36.7	36.1	35.4	35.2

4.3.3 Static Colors and Multi-plane Coefficient

To validate the contributions of static component \mathbf{K}_0^c and dynamic components ($\{\mathbf{K}_n^c(\mathbf{x})\}_{n=1}^{N_{\text{basis}}}$, $\{\mathbf{K}_n^\alpha(\mathbf{x})\}_{n=1}^{N_{\text{basis}}}$, \mathcal{B}), we performed experiments without these modules. As shown in Table 4, without static component or dynamic components will lead to a worse result than the full model. We separately render the static and dynamic parts of the Temporal-MPI to prove their individual contributions. The visualization of separate rendering settings are shown in

Figure 3. It can be seen that the static components successfully capture the static energy of the video, while the dynamic components complements the static ones to produce high quality dynamic contents.

Table 4: Ablation study of static and dynamic components.

Methods	Metrics		
	SSIM (\uparrow)	PSNR (\uparrow)	LPIPS (\downarrow)
w/o static	0.592	18.9	0.426
w/o dynamic	0.613	19.3	0.213
Full	0.934	31.9	0.034

Table 5: Inference time vs. shape of Temporal-MPI.

Resolution	No.Basis	No.Planes	Inference Time (seconds, \downarrow)
596 \times 320	5	32	0.002
596 \times 320	13	32	0.003
1038 \times 1940	5	32	0.025
1038 \times 1940	13	32	0.029
1038 \times 1940	5	192	0.030

4.3.4 Inference Speed

In this section, we investigate the relationships between inference speed and the size of Temporal-MPI. From Table 5, we can find that the computations of linear combinations of basis are efficient, and a big volume size of Temporal-MPI will not affect its real-time performance. All experiments are conducted on one Nvidia Tesla V100 GPU.

4.4 Evaluation and Comparison

4.4.1 Evaluation on Compactness of Representation

To prove the efficiency and compactness of our method, we compare our method with state-of-the-art algorithms, *3DMaskVol21* [12] and *NeuralFlow21* [11], in terms of

storage space and inference speed. One of the main objectives of our approach is to learn a compact representation of a dynamic scene. So we evaluate the compactness of Temporal-MPI by comparing the number of network parameters and storage space with these two methods. As shown in Table 1, our method only requires 0.002 seconds to generate a time-instance MPI for real-time rendering, which is **three thousand times** faster than *NeuralFlow21* and **one thousand times** faster than *3DMaskVol21*; additionally, modeling a dynamic scene with 24 timestamps, Temporal-MPI only occupies 481 Mb for storage, which is **eleven times** smaller than *3DMaskVol21* on storage space. So our approach is extremely faster and compacter for real-time rendering than existing methods.

4.4.2 Evaluation on View-Synthesis Quality

We evaluate the effectiveness of our approach by comparing it to baseline methods quantitatively and qualitatively. We compare our approach with state-of-the-art single-view or multi-view novel view synthesis methods. For monocular methods, we compare with *SynSin20* [33] and *MPIs20* [32] trained on RealEstate 10K dataset [39]. *3D Photo20* [27] and *3D Ken Burns19* [21] were trained by wild images. For multi-view methods, we compare with *NeRF20* [17], *ConsisVideoDepth20* [14], *DynSyn20* [36], *NeuralFlow21* [11], *3DMaskVol21* [12] and *D-NeRF21* [23]. Some results are referenced from recent publications [11, 12]. We document the rendering quality in three error metrics: structural similarity index measure (SSIM), peak signal-to-noise ratio (PSNR), and perceptual similarity through LPIPS [38]. From Table 6, our algorithm has the highest average score across three metrics. In order to compare fairly with other methods, we resize our output image to the same resolution of *NeuralFlow21* [11] and then evaluate. Per-scene breakdown results are shown in Table 7.

A qualitative comparison can be seen in Figure 4, which shows that our method achieves best rendering quality in both static and dynamic parts. Due to the unavailability of ground truth background images, results from *3DMaskVol21* show ghosting artifacts around moving object’s boundary and fail in scenes with forward moving motions, such as jumping and umbrella.

Table 6: Quantitative evaluation of novel view synthesis on the Dynamic Scenes dataset. MV denotes whether the approach uses multi-view information or not. Experimental data are referenced from *NeuralFlow21* [11].

Methods	MV	Metrics		
		SSIM (\uparrow)	PSNR (\uparrow)	LPIPS (\downarrow)
<i>SynSin20</i> [33]	No	0.488	16.21	0.295
<i>MPIS20</i> [32]	No	0.629	19.46	0.367
<i>3D Ken Burns19</i> [21]	No	0.630	19.25	0.185
<i>3D Photo20</i> [27]	No	0.614	19.29	0.215
<i>NeRF20</i> [17]	Yes	0.893	24.90	0.098
<i>ConsisVideoDepth20</i> [14]	Yes	0.746	21.37	0.141
<i>DynSyn20</i> [36]	Yes	0.761	21.78	0.127
<i>NeuralFlow21</i> [11]	Yes	0.928	28.19	0.045
<i>D-NeRF21</i> [23]	Yes	0.334	17.05	0.545
<i>3DMaskVol21</i> [12]	Yes	0.603	20.10	0.285
Ours	Yes	0.934	31.19	0.034

Table 7: Per-scene breakdown results from *DynSyn20*’s Dynamic Scenes dataset.

Scene	Metrics		
	PSNR(\uparrow)	SSIM(\uparrow)	LPIPS(\downarrow)
Skating-2	36.206	0.967	0.169
Balloon1-2	31.220	0.942	0.033
DynamicFace-2	28.847	0.957	0.032
Jumping	31.649	0.942	0.030
Playground	27.874	0.915	0.043
Balloon2-2	30.870	0.940	0.023
Truck-2	33.823	0.938	0.049
Umbrella	28.998	0.873	0.045
Average	31.185	0.934	0.034

5 Concluding Remarks

5.1 Limitations

Modeling dynamic scenes is challenging due to complex motions of dynamic objects over time, and specular surface and occlusions on angular domain. Our method makes the first attempt to use a compact temporal representation to

reproduce dynamic scenes in time-sequences. Similar to *NeRF20*, our method requires optimisation for each scene. Additionally, the output resolution is limited due to limited GPU memory. Furthermore, there are trade-offs among the number of bases, memory usage, output resolution and the length of modeled sequences. The rendering quality degrades when the length of sequence increases given default model parameters, or when large motion exists.

5.2 Conclusion

We have proposed a novel dynamic scene representation on top of Multi-plane Image (MPI) with basis learning. Our representation is efficient in computing, thus allowing real-time rendering of dynamics. Extensive studies on public dataset demonstrate the state-of-the-art rendering quality and efficiency of our approach. We believe using basis learning for temporal recovery and compression can be applied to the general problem of modeling dynamic contents and not limited to MPI.

References

- [1] Antonio Agudo and Francesc Moreno-Noguer. Simultaneous pose and non-rigid shape with particle dynamics. In *CVPR*, pages 2179–2187, 2015.

- [2] Adrien Bartoli, Yan Gérard, Francois Chadebecq, Toby Collins, and Daniel Pizarro. Shape-from-template. *IEEE transactions on pattern analysis and machine intelligence*, 37(10):2099–2118, 2015.
- [3] Antonin Chambolle and Pierre-Louis Lions. Image recovery via total variation minimization and related problems. *Numerische Mathematik*, 76(2):167–188, 1997.
- [4] Anpei Chen, Zexiang Xu, Fuqiang Zhao, Xiaoshuai Zhang, Fanbo Xiang, Jingyi Yu, and Hao Su. Mvsnerf: Fast generalizable radiance field reconstruction from multi-view stereo. *arXiv preprint:2103.15595*, 2021.
- [5] Ronghang Hu, Nikhila Ravi, Alexander C. Berg, and Deepak Pathak. Worldsheet: Wrapping the world in a 3d sheet for view synthesis from a single image. In *ICCV*, pages 12528–12537, 2021.
- [6] Eddy Ilg, Nikolaus Mayer, Tonmoy Saikia, Margret Keuper, Alexey Dosovitskiy, and Thomas Brox. FlowNet 2.0: Evolution of optical flow estimation with deep networks. In *CVPR*, pages 2462–2470, 2017.
- [7] Hae Gon Jeon, Jaesik Park, Gyeongmin Choe, Jinsun Park, Yunsu Bok, Yu Wing Tai, and In So Kweon. Accurate depth map estimation from a lenslet light field camera. In *CVPR*, pages 1547–1555, 2015.
- [8] Jing Jin, Junhui Hou, Jie Chen, Huanqiang Zeng, Sam Kwong, and Jingyi Yu. Deep coarse-to-fine dense light field reconstruction with flexible sampling and geometry-aware fusion. *IEEE Transactions on Pattern Analysis and Machine Intelligence*, pages 1–1, 2020.
- [9] Nima Khademi Kalantari, Ting-Chun Wang, and Ravi Ramamoorthi. Learning-based view synthesis for light field cameras. *ACM Transactions on Graphics*, 35(6):1–10, 2016.
- [10] Tianye Li, Mira Slavcheva, Michael Zollhoefer, Simon Green, Christoph Lassner, Changil Kim, Tanner Schmidt, Steven Lovegrove, Michael Goesele, and Zhaoyang Lv. Neural 3d video synthesis. *arXiv preprint:2103.02597*, 2021.
- [11] Zhengqi Li, Simon Niklaus, Noah Snavely, and Oliver Wang. Neural scene flow fields for space-time view synthesis of dynamic scenes. In *CVPR*, pages 6498–6508, 2021.
- [12] Kai-En Lin, Lei Xiao, Feng Liu, Guowei Yang, and Ravi Ramamoorthi. Deep 3d mask volume for view synthesis of dynamic scenes. In *ICCV*, pages 1749–1758, 2021.
- [13] Guangcan Liu, Zhouchen Lin, Shuicheng Yan, Ju Sun, Yong Yu, and Yi Ma. Robust recovery of subspace structures by low-rank representation. *IEEE transactions on pattern analysis and machine intelligence*, 35(1):171–184, 2012.
- [14] Xuan Luo, Jia-Bin Huang, Richard Szeliski, Kevin Matzen, and Johannes Kopf. Consistent video depth estimation. *ACM Transactions on Graphics*, 39(4), 2020.
- [15] Leonard McMillan and Gary Bishop. Plenoptic modeling: An image-based rendering system. In *Proceedings of the 22nd annual conference on Computer graphics and interactive techniques*, pages 39–46, 1995.
- [16] Ben Mildenhall, Pratul P. Srinivasan, Rodrigo Ortiz-Cayon, Nima Khademi Kalantari, Ravi Ramamoorthi, Ren Ng, and Abhishek Kar. Local light field fusion: Practical view synthesis with prescriptive sampling guidelines. *ACM Transactions on Graphics*, 38(4):1–14, 2019.
- [17] Ben Mildenhall, Pratul P. Srinivasan, Matthew Tancik, Jonathan T. Barron, Ravi Ramamoorthi, and Ren Ng. Nerf: Representing scenes as neural radiance fields for view synthesis. In *ECCV*, pages 405–421, 2020.
- [18] Francesc Moreno-Noguer and Pascal Fua. Stochastic exploration of ambiguities for nonrigid shape recovery. *IEEE transactions on pattern analysis and machine intelligence*, 35(2):463–475, 2012.
- [19] J. Navarro and A. Buades. Robust and dense depth estimation for light field images. *IEEE Transactions on Image Processing*, 26(4):1873–1886, 2017.
- [20] Ren Ng, Marc Levoy, Mathieu Brédif, Gene Duval, Mark Horowitz, and Pat Hanrahan. *Light field photography with a hand-held plenoptic camera*. PhD thesis, Stanford University, 2005.
- [21] Simon Niklaus, Long Mai, Jimei Yang, and Feng Liu. 3d ken burns effect from a single image. *ACM Transactions on Graphics*, 38(6), 2019.
- [22] Thomas Porter and Tom Duff. Compositing digital images. *SIGGRAPH Comput. Graph.*, 18(3):253–259, 1984.
- [23] Albert Pumarola, Enric Corona, Gerard Pons-Moll, and Francesc Moreno-Noguer. D-nerf: Neural radiance fields for dynamic scenes. In *CVPR*, pages 10318–10327, 2021.
- [24] René Ranftl, Katrin Lasinger, David Hafner, Konrad Schindler, and Vladlen Koltun. Towards robust monocular depth estimation: Mixing datasets for zero-shot cross-dataset transfer. *IEEE Transactions on Pattern Analysis and Machine Intelligence*, page 1, 2020.
- [25] Johannes Lutz Schönberger and Jan-Michael Frahm. Structure-from-motion revisited. In *CVPR*, pages 4104–4113, 2016.
- [26] Jonathan Shade, Steven Gortler, Li-wei He, and Richard Szeliski. Layered depth images. In *ACM SIGGRAPH*, pages 231–242, 1998.
- [27] Meng-Li Shih, Shih-Yang Su, Johannes Kopf, and Jia-Bin Huang. 3D photography using context-aware layered depth inpainting. In *CVPR*, pages 8025–8035, 2020.

- [28] Vincent Sitzmann, Justus Thies, Felix Heide, Matthias Nießner, Gordon Wetzstein, and Michael Zollhöfer. Deepvoxels: Learning persistent 3d feature embeddings. In *CVPR*, pages 2437–2446, 2019.
- [29] Pratul P Srinivasan, Tongzhou Wang, Ashwin Sreelal, Ravi Ramamoorthi, and Ren Ng. Learning to synthesize a 4D RGBD light field from a single image. In *ICCV*, pages 2243–2251, 2017.
- [30] Chengzhou Tang, Lu Yuan, and Ping Tan. Lsm: Learning subspace minimization for low-level vision. In *CVPR*, pages 6235–6246, 2020.
- [31] Carlo Tomasi and Takeo Kanade. Shape and motion from image streams under orthography: a factorization method. *International journal of computer vision*, 9(2):137–154, 1992.
- [32] Richard Tucker and Noah Snavely. Single-view view synthesis with multiplane images. In *CVPR*, pages 551–560, June 2020.
- [33] Olivia Wiles, Georgia Gkioxari, Richard Szeliski, and Justin Johnson. SynSin: End-to-end view synthesis from a single image. In *CVPR*, pages 7465–7475, 2020.
- [34] Suttisak Wizatwongsa, Pakkapon Phongthawee, Jiraphon Yenphraphai, and Supasorn Suwajanakorn. Nex: Real-time view synthesis with neural basis expansion. In *CVPR*, pages 8534–8543, 2021.
- [35] Jonas Wulff and Michael J Black. Efficient sparse-to-dense optical flow estimation using a learned basis and layers. In *CVPR*, pages 120–130, 2015.
- [36] Jae Shin Yoon, Kihwan Kim, Orazio Gallo, Hyun Soo Park, and Jan Kautz. Novel view synthesis of dynamic scenes with globally coherent depths from a monocular camera. In *CVPR*, pages 5336–5345, 2020.
- [37] Alex Yu, Ruilong Li, Matthew Tancik, Hao Li, Ren Ng, and Angjoo Kanazawa. Plenotrees for real-time rendering of neural radiance fields. *arXiv preprint:2103.14024*, 2021.
- [38] Richard Zhang, Phillip Isola, Alexei A Efros, Eli Shechtman, and Oliver Wang. The unreasonable effectiveness of deep features as a perceptual metric. In *CVPR*, pages 586–595, 2018.
- [39] Tinghui Zhou, Richard Tucker, John Flynn, Graham Fyffe, and Noah Snavely. Stereo magnification: Learning view synthesis using multiplane images. *ACM Transactions on Graphics*, 37(4):1–12, 2018.

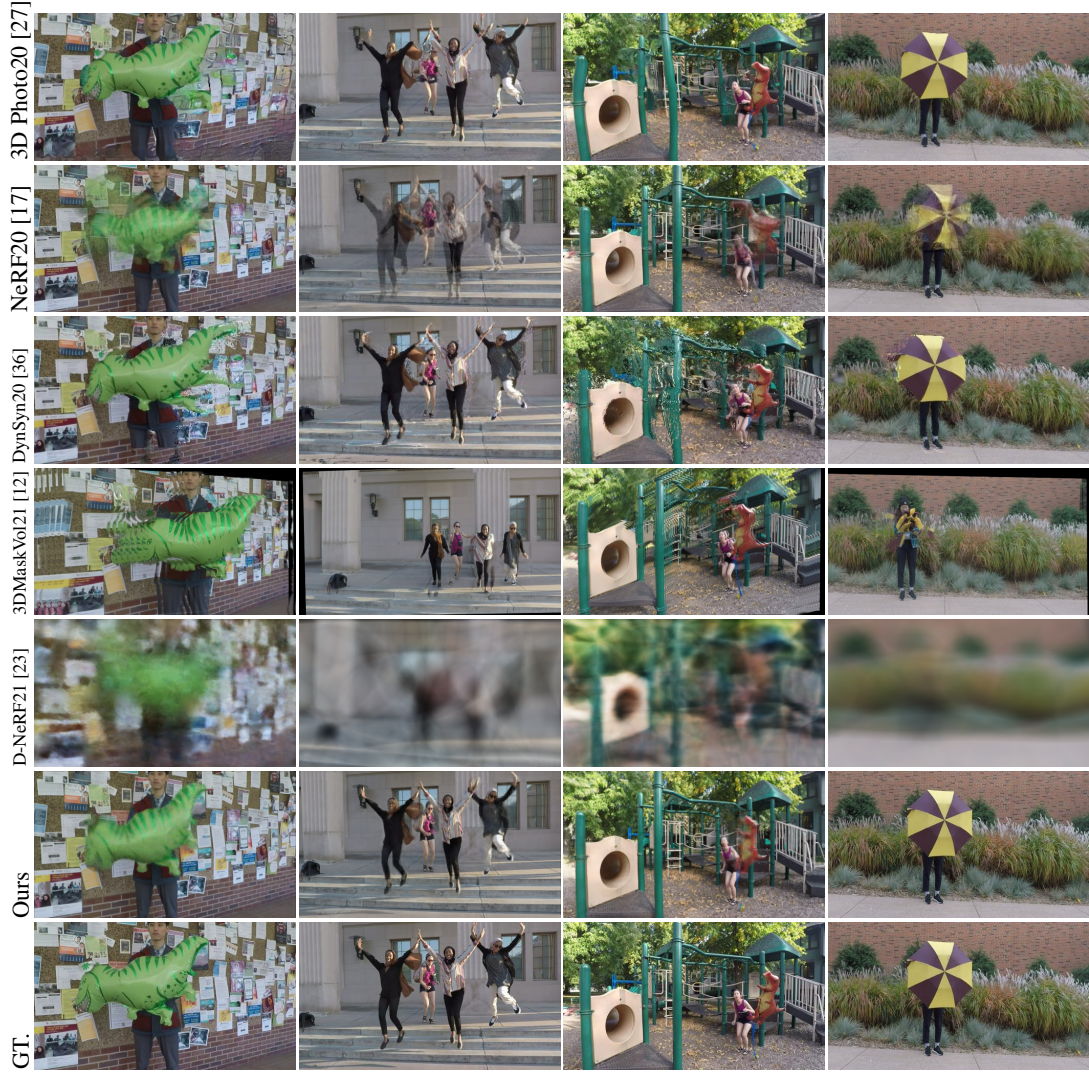


Figure 4: Qualitative comparisons on the Dynamic Scenes dataset. The visual results of *3D Photo20*, *NeRF20* and *DynSyn20* are referenced from [11]. Observed from above images, *D-NeRF21* produces blurry results, *DynSyn20* has great artifacts on thin structures, *3D Photo20* generates distortions, *3DMaskVol21* produces ghosting effects around the object’s boundary.